

# Diquark Substructure in $\phi$ Photoproduction

Richard F. Lebed\*

Department of Physics, Arizona State University, Tempe, Arizona 85287-1504, USA

(Dated: October, 2015)

Observed enhancements in the forward and backward directions for  $\phi$  meson photoproduction off nucleons are shown to be explainable by the production of a nonresonant recoiling ( $su$ ) diquark, ( $\bar{s}ud$ ) triquark pair. We show that the necessity of maintaining approximate collinearity of the quarks within these units constrains configurations with the minimum momentum transfer, and hence maximal amplitudes, to lie preferentially along the reaction axis.

PACS numbers: 14.20.Pt, 12.39.Mk, 12.39.-x

Keywords: exotic baryons; pentaquarks; diquarks

## I. INTRODUCTION

LHCb has recently observed [1] two exotic states,  $P_c^+(4380)$  and  $P_c^+(4450)$ , at high significance in the  $J/\psi$  spectrum of  $\Lambda_b \rightarrow J/\psi K^- p$ . In addition to extracting the state masses and widths, the collaboration also measured the phases of the production amplitude and found them to be compatible with genuine resonant behavior. Such properties strongly support the assertion that true pentaquark states have at last been revealed. Should the  $P_c^+$  states be confirmed at another experiment, they will join  $X$ ,  $Y$ , and  $Z$  exotic mesons (widely believed to have valence tetraquark structure) as the first hadrons observed at high significance to lie outside of the textbook  $q\bar{q}$ -meson,  $qqq$ -baryon paradigm.

Of particular note is that all of the observed exotic states contain  $c\bar{c}$  (or  $b\bar{b}$ ) pairs. The possibility of light-flavor ( $u, d, s$ ) tetraquarks or pentaquarks has been discussed for decades, but despite intense experimental efforts, no unambiguous signal of such a state has ever survived scrutiny. Nor has a singly-heavy hadron ( $D_s$ ,  $\Lambda_b$ , etc.) been identified as unambiguously exotic. One possible explanation for this first appearance in doubly-heavy channels, as argued implicitly in Ref. [2] and explicitly in Refs. [3, 4], is that the exotic consists of two components, each of which contains a heavy quark and therefore is fairly compact, and which are separated from each other in the sense of having a suppressed large wave function overlap. Such a configuration is much more difficult to realize with light quarks. While this scenario could be achieved by hadronic molecules (for instance, if the famous  $X(3872)$  tetraquark candidate has a  $c\bar{c}u\bar{u}$  valence-quark structure organized into a  $D^0\bar{D}^{*0}$  molecule), in this paper we use the innovation of Ref. [2] to assert the existence of hadrons formed of separating *colored* components that are individually held together by the attractive  $\mathbf{3} \otimes \mathbf{3} \supset \mathbf{3}$  color interaction, and collectively prevented from separating asymptotically far due to color confinement.

If the existence of observable exotics is contingent upon

each of its components containing a heavy quark, then one may hope that some vestige of the exotic behavior persists in analogous production mechanisms with valence  $s\bar{s}$  rather than  $c\bar{c}$  ( $b\bar{b}$ ) quark pairs. In Ref. [2], the observed tetraquark states were argued to arise from a rapidly separating diquark-antidiquark pair,  $(cq)_{\mathbf{3}}(\bar{c}\bar{q}')_{\mathbf{3}}$  ( $q$  in the following generically indicates  $u$  or  $d$  quarks) that subsequently hadronizes only through the large- $r$  tails of meson wave functions stretching from the quarks in the diquarks to the antiquarks in the antidiquarks. This picture was extended in Ref. [4] to explain the pentaquark states as an analogous diquark-antitriquark pair (this combination having been first proposed for lighter-quark pentaquarks in Ref. [5]),  $(cu)_{\mathbf{3}}[\bar{c}(ud)_{\mathbf{3}}]_{\mathbf{3}}$ , where the  $(ud)$  diquark is inherited from the parent  $\Lambda_b$  baryon, and the triquark is seen to assemble from a further  $\mathbf{3} \otimes \mathbf{3} \supset \mathbf{3}$  attraction. A short review of these papers appears in Ref. [6]. If this mechanism produces such prominent effects in the  $c\bar{c}$  system as pentaquark resonances, then one may hope to see at least a remnant of the mechanism in the  $s\bar{s}$  system, in the form of peculiar features appearing in the data.

Shortly after the LHCb announcement, multiple theoretical papers appeared, discussing various interpretations of the  $P_c^+$  states and advocating for experiments in which to study them. Among the latter, three separate collaborations [7–9] proposed using  $\gamma N \rightarrow P_c \rightarrow J/\psi N^{(*)}$  photoproduction of nucleons  $N$  as sensitive tests of the internal structure of the  $P_c$  states. In each case, the  $c\bar{c}$  pair arises through the dissociation of the incoming photon. By the reasoning of the previous paragraph, one may therefore ask if any unusual features have arisen in the analogous  $s\bar{s}$  process of  $\phi$  photoproduction,  $\gamma p \rightarrow \phi p$ .

In fact, a detailed experimental study of  $\phi$  photoproduction was also published fairly recently by the CLAS Collaboration at Jefferson Lab [10]. Data in the neutral ( $K_L K_S$ ) mode are presented in Ref. [11]. The most interesting feature in the cross section data is a forward-angle “bump” structure at  $\sqrt{s} \approx 2.2$  GeV (about 250 MeV above threshold) that rises about a factor 2–3 above a more mildly varying curve in  $\sqrt{s}$ . However, this structure appears only at the most forward angles (in which  $\phi$  lies in the same direction as  $\gamma$  in the center-of-momentum [c.m.] frame), and as argued in Ref. [12], such a unidi-

\*Electronic address: richard.lebed@asu.edu

rectional structure almost certainly does not indicate a resonance. In addition, the cross section data indicate a small but clear increase at the most backward angles (a factor of perhaps 50 smaller than the forward peak<sup>1</sup>); while Ref. [10] mentions a possible origin for backward enhancement in the  $u$ -channel exchange of a nucleon, they also comment that such a direct  $\phi$ - $p$  coupling would require a nucleon strangeness content or a violation of OZI suppression surprisingly larger than expected.

Here we argue that both features can be explained in a very simple way: A fraction of  $\phi$  photoproduction events proceed through a constituent exchange between the  $\gamma$  (dissociated into an  $s\bar{s}$  state) and the nucleon [treated as a bound state of a  $(ud)$  diquark and a light quark  $q$ ] (Fig. 1). The scattering products are a diquark-antitriquark pair,  $(sq)_{\mathbf{3}}[\bar{s}(ud)_{\mathbf{3}}]_{\mathbf{3}}$ , completely analogous to the construction proposed for the  $P_c^+$  resonances, but as experiment indicates, nonresonant in this case. That

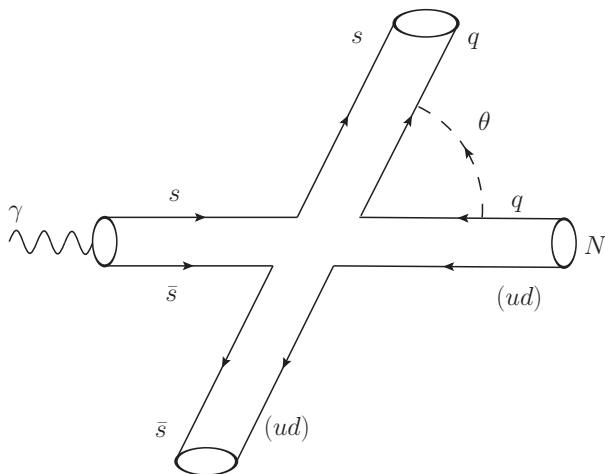


FIG. 1: The constituent exchange for  $\phi$  photoproduction via creation of an  $(sq)_{\mathbf{3}}$  diquark- $[\bar{s}(ud)_{\mathbf{3}}]_{\mathbf{3}}$  antitriquark pair.

is, the anomalies correspond to “would-be” pentaquarks. The enhancement in the forward and backward directions, with the forward direction favored, is explained by the preference of the diquark and triquark to minimize momentum transfer by aligning with the  $\gamma p$  process axis.

This paper is organized as follows: In Sec. II we discuss the forward-backward enhancement of hadronic cross sections driven by constituent-exchange momentum transfers. A simple model based upon minimal gluon exchanges is presented in Sec. III, and the calculation and results are presented in Sec. IV. Section V summarizes and concludes.

## II. MOMENTUM TRANSFER ENHANCEMENT

One of the quintessential triumphs of quantum field theory is its natural prediction of a Rutherford-type differential scattering cross section, in which the invariant amplitude  $\mathcal{M}$  for the process  $p_1 p_2 \rightarrow p'_1 p'_2$  (using momenta to label the particles) scales as the inverse of the 4-momentum transfer  $t = q^2 = (p'_1 - p_1)^2 = (p_2 - p'_2)^2$ . A dependence  $\mathcal{M} \propto 1/(q^2 - m^2)$  arises from the virtual exchange of a quantum of mass  $m$  of the mediating interaction. For example, in  $pp$  elastic scattering the quantum (at least at low energies) may be considered a single neutral virtual meson, such as  $\pi^0$ . At higher energies, the relevant degrees of freedom exchanged become quarks and gluons.

Elastic scattering via mediators of negligible mass also features the characteristic Rutherford angular dependence  $1/q^2 \propto 1/\sin^2(\theta/2)$ , where  $\theta$  is the c.m. scattering angle. Inelastic  $2 \rightarrow 2$  scattering (and scattering with heavier mediators) also contains this factor, although the relation is then no longer a strict proportionality, and the effect is muted. In either case, however, the  $\sin^2(\theta/2)$  factor indicates strong peaking of  $\mathcal{M}$  in the forward direction, and for precisely the reason that Rutherford understood: Greater particle deflections demand stronger forces, requiring scattering events that, for given fixed initial-particle energies, are comparatively rarer. If the scattered particles  $p'_1, p'_2$  cannot be unambiguously associated with the initial particles  $p_1, p_2$ , respectively—as occurs either if  $p_1, p_2$  represent identical particles, or if the reaction is sufficiently inelastic that the association is less than perfect—then one also expects an enhancement in  $\mathcal{M}$  corresponding to the minimization of the 4-momentum transfer  $u = (p'_2 - p_1)^2 = (p_2 - p'_1)^2$ .  $u$  contains the factor  $\cos^2(\theta/2)$ , which means that  $\mathcal{M}$  also peaks in the backward direction.

A prominent and historically important example of this forward-backward peaking occurs in  $pn$  elastic scattering. Indeed, the strong backward peak, now understood to be due to the charge-exchange reaction  $p \leftrightarrow n$  in which charged mesons are traded between the nucleons, is one of the best pieces of evidence for strong interactions respecting fundamental isospin symmetry, particularly the equivalence of  $p$  and  $n$  under strong interactions: In  $pn$  scattering the backward peak is almost as high as the forward peak, because  $p$  turns into  $n$  and vice versa but remains otherwise undeflected. It is interesting to note (as discussed, *e.g.*, in Ref. [13]) that simple one-pion exchange, which one might naively expect to be responsible for the full peak, is actually well known to lead to a zero differential cross section at  $180^\circ$ . At the constituent level, a quark exchange  $u \leftrightarrow d$  occurs.

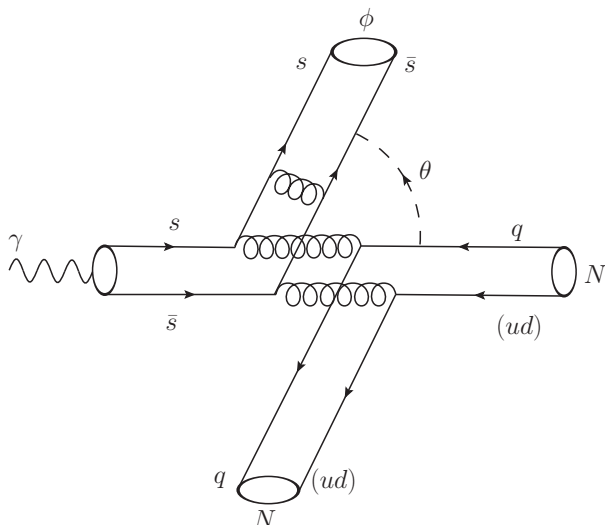
For inelastic processes, the rule of thumb for estimating the relative height of the forward and backward peaks appears to follow from the similarity of the initial and final particles. Taking  $p_1$  ( $p'_1$ ) to be the lighter initial (final) particle, one expects the forward peak to be generically higher. As an explicit example, consider  $K\Lambda$  photopro-

<sup>1</sup> M. Dugger, private communication.

duction; here,  $p_1 = \gamma \rightarrow s\bar{s}$ ,  $p'_1 = K^+$ ,  $p_2 = p$ , and  $p'_2 = \Lambda$ . The recent CLAS data for this process [14] shows a backward peak in the differential cross section that is a factor of a few smaller than the forward peak (the ratio depending strongly upon  $\sqrt{s}$ , reaching a maximum of about 1/2 around 2.1 GeV), supporting the general dynamical picture described here. Indeed, a small modification of Fig. 1 provides a simple quark-exchange picture for  $K\Lambda$  photoproduction: Just exchange  $s \leftrightarrow \bar{s}$ . The preference of forward ( $\theta \rightarrow 0$ ) scattering indicates the relative dynamical preference for not diverting the (heavier) baryon line. Alternately, at the constituent level for  $K\Lambda$  one sees that the lightest constituent  $q$  (and  $s$ ) suffers a backward scattering for  $\theta \rightarrow 0$ , while the heavier ( $ud$ ) diquark (and  $\bar{s}$ ) remains undeflected. Nevertheless, one expects a smaller enhancement for  $\theta \rightarrow \pi$  as well, where the momentum transfers of  $q$  and  $s$  are minimized.

### III. A SIMPLE DIQUARK-TRIQUARK MODEL

Once the scattered particles in a  $2 \rightarrow 2$  process are resolved into constituents, the overall momentum transfer  $q^2$  is no longer the only independent kinematical quantity contributing to angular dependence. The dominant diagram for  $\gamma N \rightarrow \phi N$  is generally attributed to Pomeron exchange [15, 16], in which the  $\gamma$  dissociates into the  $s\bar{s}$  pair.<sup>2</sup> At the level of fundamental QCD, the corresponding Feynman diagrams include as their most simple representative Fig. 2, although the full Pomeron would include many more gluons, particularly those cross-linking the exchanged gluon pair in this figure. The gluon ex-



<sup>2</sup> Alternate diagrams are possible in which  $\gamma$  couples directly to the  $N$ , and the  $s\bar{s}$  pair is created from gluons emitted from the struck  $N$ . At high energies, the latter diagram actually appears to be dominant [17].

FIG. 2: One of many gluon-exchange Feynman diagrams contributing to the Pomeron exchange mechanism for  $\gamma N \rightarrow \phi N$ .

changed between the final-state  $s\bar{s}$  pair merely indicates that, in order for the four constituents to interact, share momentum, and be diverted to their final directions, a minimum of three gluons must be exchanged<sup>3</sup>. In fact, the complete diagrams are even more complicated than indicated because we have represented the nucleon  $N$  as a bound pair of a light quark  $q$  and a diquark ( $ud$ ); indeed, the gluons can couple separately to either of the quarks in ( $ud$ ), the nucleon can contain both scalar and vector diquarks, and the quark  $q$  must be properly antisymmetrized with the identical quark in ( $ud$ ) to satisfy Fermi statistics [18]. Nevertheless, Fig. 2 illustrates the central point that the Pomeron carries the entirety of the momentum transfer  $q^2$  in the  $t$ -channel, suggesting (as is observed) strong forward peaking of the differential cross section, while a  $u$ -channel backward peak would require a complicated intermediate state carrying not only a Pomeron, but also nonzero baryon number and hidden strangeness.

We propose an additional mechanism for  $\phi$  photoproduction, namely, the production of an ( $sq$ ) color- $\bar{\mathbf{3}}$  bound diquark  $\delta$  and an [ $\bar{s}(ud)$ ] color- $\mathbf{3}$  bound antitriquark  $\bar{\theta}$ , as in Fig. 1. In this case, ( $ud$ ) truly does refer to a diquark component in  $N$ , which at first blush can be either of the “good” (scalar-isoscalar) or “bad” (vector-isovector) variety, although data from charge and magnetic nucleon radii prefer the “good” component [18], once proper antisymmetrization of the wave function between  $q$  and ( $ud$ ) is performed. In comparison, in the case of  $K\Lambda$  photoproduction described above, the  $\Lambda$  contains only the “good” ( $ud$ ) diquark. The importance of including diquark baryon substructure in AdS/QCD models to obtain Regge trajectories matching those of mesons (as is observed), is emphasized in Refs. [19, 20].

Since both  $\delta$  and  $\bar{\theta}$  are colored objects, hadronization of the pair is accomplished as in Refs. [2, 4], by means of the hadron wave functions stretching across the space between the colored bound states. One can obtain in this way not only a  $\phi = (\bar{s}s)$ ,  $N = q(ud)$  final state, but also a contribution to the final state  $K = (\bar{s}q)$ ,  $\Lambda = s(ud)$  expected to be smaller than the one discussed in the previous section, due to the smaller strength of the  $\mathbf{3} \otimes \mathbf{3} \supset \bar{\mathbf{3}}$  attraction compared to that of  $\mathbf{3} \otimes \mathbf{3} \supset \mathbf{1}$ .

Our purpose is not to calculate the complete amplitude for this entire process (*e.g.*, the techniques of Ref. [21] are useful for the large- $\theta$  region), but only to demonstrate that a natural physical mechanism exists to provide an interaction producing an enhanced cross section in both the forward and backward directions. We can therefore make a number of simplifying assumptions. First, we ne-

<sup>3</sup> Note that the ( $ud$ ) is treated as a single unit in the scattering.

glect Fermi motion within the  $\delta$  and  $\bar{\theta}$ , so that the constituents within each bound state move with the same velocity (this assumption can be lifted by folding in appropriate distribution functions; *e.g.*, in the light-front formalism, see Ref. [22]). Then it is clear from Fig. 1 that forward ( $\theta \rightarrow 0$ ) scattering of  $(sq)$  also produces a forward-scattered  $\phi$ , since in the c.m.  $(sq)$  and  $[\bar{s}(ud)]$  have the same momentum magnitude, but the former is lighter and therefore has a larger speed. In turn,  $s$  has a larger speed than  $\bar{s}$ . Since  $m_s = m_{\bar{s}}$ , the net momentum of  $\phi = (s\bar{s})$  then points in the same direction as  $s$ , and hence, as  $(sq)$ .

This strategy has much in common with the “hard scattering approach” (HSA) developed in Refs. [23, 24], in that both take all constituents to move collinear with their parent hadrons, include the minimal necessary number of gluon exchanges to accomplish the process, and require folding in appropriate distribution amplitudes. The HSA approach applied to  $\phi$  photoproduction at high energy scales (with genuinely hard gluons) has been studied in Ref. [17], although using older data than here.

Since the diagrams again have four constituents, the minimum number of gluon exchanges necessary for the process remains three. Unlike in Pomeron exchange, however, the  $\delta$ - $\bar{\theta}$  production mechanism provides natural alternatives that produce enhancements in the forward and backward directions. Consider first Fig. 3; here, the scattering process is driven by the lightest constituent ( $q$ ) from either of the initial particles ( $N$ ) exchanging a gluon with the  $\bar{s}$  constituent of the other initial particle ( $\gamma$ ). As

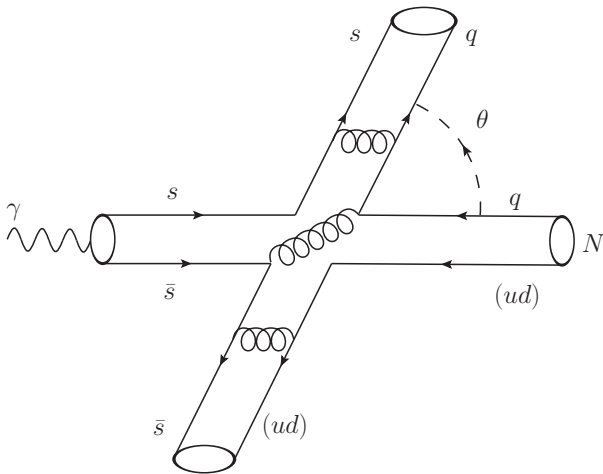


FIG. 3: As in Fig. 1, but including a minimal gluon exchange that naturally explains the enhancement of  $\phi$  production in the  $\theta \rightarrow 0$  direction, as described in the text.

just discussed, the  $\delta$ - $\bar{\theta}$  configuration favored for forward  $\phi$  production is the one in which  $(sq)$  is also produced in the forward direction, recoiling against  $[\bar{s}(ud)]$ . Since the lightest constituent (here,  $q$ ) is the easiest to deflect through large angles, this particular exchange diagram provides a natural mechanism for backward scattering of

the  $q$ , as well as that of the  $\bar{s}$ .

Once the  $q$  and  $\bar{s}$  are deflected through a large angle, the  $s$  and  $(ud)$  must each be deflected (through a generically smaller angle) to become bound to into their respective  $(sq)$  and  $[\bar{s}(ud)]$  combinations. This binding is accomplished in our crude picture by the exchange of a gluon between  $s$  and  $q$ , and between  $\bar{s}$  and  $(ud)$ , as depicted in Fig. 3. As promised, the minimal number of gluon exchanges required to achieve the desired final states is precisely three. One therefore naively expects this diagram to peak in the forward direction, and in the next section we see this expectation indeed to be realized.

A natural exchange diagram producing a backward peak is depicted in Fig. 4. Here, the interaction gluon connects the heaviest component  $[(ud)]$  to the  $s$ , and is

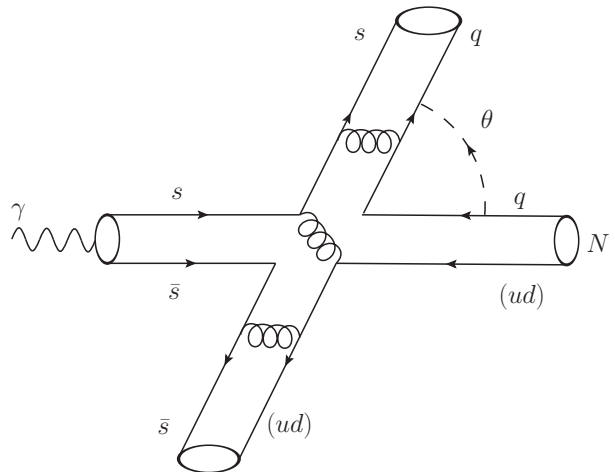


FIG. 4: As in Fig. 1, but including a minimal gluon exchange that naturally explains the enhancement of  $\phi$  production in the  $\theta \rightarrow \pi$  direction, as described in the text. The angle  $\theta$  exhibited here is identical to the one in Fig. 3, for the purpose of ease of comparison.

expected to produce an enhancement when both of them are deflected in the backward direction, the  $\theta \rightarrow \pi$  limit of Fig. 4. In that case, in order to form the  $[\bar{s}(ud)]$  and  $(sq)$  combinations, the  $\bar{s}$  and  $q$  deflect through a smaller angle, and binding is accomplished through gluon exchanges between  $(ud)$  and  $\bar{s}$ , and between  $s$  and  $q$ , respectively. Again, a minimum of precisely three gluon exchanges is necessary to obtain the desired final state. And since backward deflection of the heavier  $(ud)$  is not as easy as backward deflection of the lighter  $q$ , one expects the size of the enhancement in the backward direction produced by Fig. 4 to be smaller than the enhancement in the forward direction produced by Fig. 3, which is verified in the next section to be true.

Before proceeding to a calculation, we hasten to emphasize its extremely rudimentary nature. First, we are investigating a particular production mechanism ( $\delta$ - $\bar{\theta}$ ) that has never been demonstrated unambiguously to occur in any process. The  $(sq)$  and  $[\bar{s}(ud)]$  are assumed

to act as bound quasiparticles, allowing for analysis as a  $2 \rightarrow 2$  process. Second, we suppose that the reaction proceeds through a “good” diquark component of the nucleon, which interacts as a unit and maintains its identity throughout the process. Third, we neglect the Fermi motion of each composite particle and assume that each initial and final state consists of two collinear components moving at the same velocity. Fourth, we use the minimum required number of gluons for each process, despite the fact that the reaction and binding interactions are most certainly nonperturbative. No hard scale is present to justify a perturbative treatment, and the gluons here should be thought of only as quasiparticles that accomplish momentum transfer among the components; in reality, these gluons simply represent collections of multiple gluon exchanges that accomplish the same overall scattering. In fact, the specific choices of topology for the diagrams in Figs. 3, 4, even with the minimal gluon exchange number, are not unique. For example, while it is tempting to apply the above narrative that the interaction between some of the constituents occurs first, and then the remaining constituents exchange gluons with the scattered components to form bound states, it is just as tenable from a quantum field-theory point of view that the initial constituents  $\gamma$  and  $N$  come unbound by gluon exchange first, and then the interaction occurs. Or, the binding and unbinding gluons can stretch across the interaction<sup>4</sup>. In real QCD, one expects *all* such gluons to appear—copiously—in a typical diagram.

To establish a systematic calculation, we consider all 12 diagrams that have the minimum three planar gluons, such that each of the constituents must couple at least once to a gluon. Figures 3 and 4 may be considered as representatives of diagram classes [with amplitudes  $\mathcal{M}^{(1)}$  and  $\mathcal{M}^{(2)}$ , respectively], as defined by the placement of the central interaction gluon that connects initial and final states. The members of each class are defined by which two external states have their constituents connected by a gluon. In a third allowed class represented by Fig. 5 [amplitudes  $\mathcal{M}^{(3)}$ ], the constituents of each of three of the external states are connected by a gluon. The definition of the 12 diagrams is summarized in Table I; thus, for example, the amplitudes corresponding to the literal diagrams of Figs. 3, 4, and 5 are  $\mathcal{M}_1^{(1)}$ ,  $\mathcal{M}_1^{(2)}$ , and  $\mathcal{M}_1^{(3)}$ , respectively. It is also simple to check that each of these 12 diagrams also has exactly two internal constituent propagators.

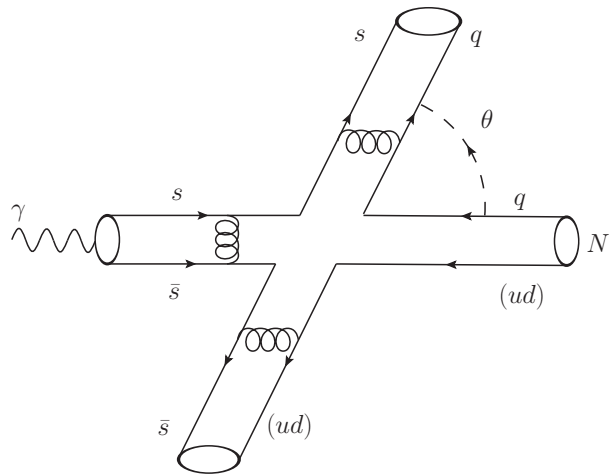


FIG. 5: As in Fig. 1, but including a minimal gluon exchange that does not have a natural central interaction gluon connecting initial and final states.

TABLE I: Amplitudes based on the classes defined by Figs. 3, 4, 5 [defined as  $\mathcal{M}^{(1),(2),(3)}$ , respectively]. Each amplitude is defined by its class and the listed subset of initial and final states, each member of which exchanges a single binding gluon.

$\mathcal{M}_1^{(1)}$ ( $\delta, \bar{\theta}$ )	$\mathcal{M}_1^{(2)}$ ( $\delta, \bar{\theta}$ )	$\mathcal{M}_1^{(3)}$ ( $\gamma, \delta, \bar{\theta}$ )
$\mathcal{M}_2^{(1)}$ ( $\gamma, N$ )	$\mathcal{M}_2^{(2)}$ ( $\gamma, N$ )	$\mathcal{M}_2^{(3)}$ ( $N, \delta, \bar{\theta}$ )
$\mathcal{M}_3^{(1)}$ ( $\delta, N$ )	$\mathcal{M}_3^{(2)}$ ( $\delta, \gamma$ )	$\mathcal{M}_3^{(3)}$ ( $\gamma, N, \delta$ )
$\mathcal{M}_4^{(1)}$ ( $\gamma, \bar{\theta}$ )	$\mathcal{M}_4^{(2)}$ ( $N, \bar{\theta}$ )	$\mathcal{M}_4^{(3)}$ ( $\gamma, N, \bar{\theta}$ )

#### IV. CALCULATION AND RESULTS

We estimate the relative size of the diagrams in Table I by establishing kinematics and definitions of momenta, and then by calculating the angular dependence originating from the product of momentum transfer factors forming the denominators of the three gluon propagators and two constituent propagators appearing in each diagram. Spin structures in the form of Dirac matrices or Lorentz tensors are also ignored; indeed, the issue of how to parametrize the coupling of a gluon to the  $(ud)$  diquark is avoided with this assumption. The precise recipe for treating masses appearing in these factors is described below. In short, we estimate the relative sizes and angular dependences of the 12 amplitudes  $\mathcal{M}$  in Table I by using just a few of the factors appearing in each of them.

We begin with kinematical conventions. The external composite particle masses, not only  $m_\gamma = 0$  and  $m_p$ , but also the diquark  $m_{(sq)}$  and antitriple quark  $m_{[\bar{s}(ud)]}$  masses, are assumed known, uniquely determining the c.m. energy and momenta of the external particles in terms of the total c.m. energy  $\sqrt{s}$  of the process, as in any  $2 \rightarrow 2$

<sup>4</sup> Such gluons would be nonplanar, and give contributions formally suppressed by  $O(1/N_c^2)$  relative to diagrams without them, where  $N_c = 3$  is the number of QCD colors.

process:

$$\begin{aligned}
\sqrt{s} = E_{\text{tot}}^{\text{c.m.}} &= \sqrt{m_N(2E_\gamma^{\text{lab}} + m_N)}, \\
E_\gamma^{\text{c.m.}} &= \frac{s - m_N^2}{2\sqrt{s}}, \\
E_N^{\text{c.m.}} &= \frac{s + m_N^2}{2\sqrt{s}}, \\
p_\gamma^{\text{c.m.}} = p_N^{\text{c.m.}} &= E_\gamma^{\text{c.m.}}, \\
E_{(sq)}^{\text{c.m.}} &= \frac{s - m_{[\bar{s}(ud)]}^2 + m_{(sq)}^2}{2\sqrt{s}}, \\
E_{[\bar{s}(ud)]}^{\text{c.m.}} &= \frac{s - m_{(sq)}^2 + m_{[\bar{s}(ud)]}^2}{2\sqrt{s}}, \quad (1)
\end{aligned}$$

and

$$\begin{aligned}
p_{(sq)}^{\text{c.m.}} = p_{[\bar{s}(ud)]}^{\text{c.m.}} = \\
\frac{\sqrt{\left[ s - (m_{[\bar{s}(ud)]} + m_{(sq)})^2 \right] \left[ s - (m_{[\bar{s}(ud)]} - m_{(sq)})^2 \right]}}{2\sqrt{s}}. \quad (2)
\end{aligned}$$

Since the constituents of each composite particle are assumed to move with the same velocity, the fraction of the total momentum carried by each is assumed to be the ratio of its mass to the total mass of the constituents. In particular, if we define

$$\begin{aligned}
r_1 &\equiv \frac{m_s}{m_s + m_{\bar{s}}}, \\
r_2 &\equiv \frac{m_q}{m_q + m_{(ud)}}, \\
r_3 &\equiv \frac{m_q}{m_s + m_q}, \\
r_4 &\equiv \frac{m_{\bar{s}}}{m_{\bar{s}} + m_{(ud)}}, \quad (3)
\end{aligned}$$

and denote initial and final constituent momenta with primes on the latter and not on the former, then

$$\begin{aligned}
p_s &= r_1 p_\gamma, \\
p_{\bar{s}} &= (1 - r_1) p_\gamma, \\
p_q &= r_2 p_N, \\
p_{(ud)} &= (1 - r_2) p_N, \\
p'_s &= (1 - r_3) p_{(sq)}, \\
p'_{\bar{s}} &= r_4 p_{[\bar{s}(ud)]}, \\
p'_q &= r_3 p_{(sq)}, \\
p'_{(ud)} &= (1 - r_4) p_{[\bar{s}(ud)]}. \quad (4)
\end{aligned}$$

This simple apportionment of momenta among constituents is completely analogous to the result in light-front quantum field theory [25]. Conservation of 4-momentum at each vertex then completely determines the momentum transfers in terms of the  $r_i$  factors and

scalar products between the external momenta, which in turn are completely determined by the external particle masses and the scattering angle  $\theta$ .

Out of the 12 diagrams, only six distinct gluon momenta appear:

$$\begin{aligned}
q_s &\equiv p'_s - p_s, \\
q_{\bar{s}} &\equiv p'_{\bar{s}} - p_{\bar{s}}, \\
q_q &\equiv p'_q - p_q, \\
q_{(ud)} &\equiv p'_{(ud)} - p_{(ud)}, \\
q_{(sq)} &\equiv p_{(sq)} - p_s - p_q = p_{\bar{s}} + p_{(ud)} - p_{[\bar{s}(ud)]}, \\
q_{s\bar{s}} &\equiv p'_s + p'_{\bar{s}} - p_\gamma = p_N - p'_q - p'_{(ud)}, \quad (5)
\end{aligned}$$

which satisfy between them three simple identities:

$$\begin{aligned}
q_{(sq)} &= q_s + q_q = -q_{\bar{s}} - q_{(ud)}, \\
q_{s\bar{s}} &= q_s + q_{\bar{s}} = -q_q - q_{(ud)}, \\
0 &= q_s + q_{\bar{s}} + q_q + q_{(ud)}, \quad (6)
\end{aligned}$$

so that only three of them are linearly independent, exactly as one expects for momentum transfers between four independent external momenta. Compared to the full Feynman calculation with gluons in the amplitudes  $\mathcal{M}$ , we treat the gluon propagator factors  $q_j^2$  as the only relevant ones for this analysis (*i.e.*, we neglect polarization tensor structures). However, using skeletal diagrams such as Figs. 3, 4, 5 to model much more complicated diagrams with extensive gluon and internal  $q\bar{q}$  exchanges introduces the potential for artificial kinematic singularities to arise when some of the internal lines go on mass shell. Part of this problem is caused by the assumption of zero transverse constituent momenta, but much of it simply is due to the usual soft-gluon infrared singularities one expects in a perturbative treatment. Physically, an on-shell gluon corresponds to an infinite-range interaction between the constituents, which does not interact with the finite range associated with confinement. To account for this important dynamics, we provide the gluons with a finite mass scale  $m_{\text{conf}}$  (with a specific value chosen below), and introduce dimensionless gluon propagator factors

$$Q_j \equiv -\frac{m_{\text{conf}}^2}{q_j^2 - m_{\text{conf}}^2}, \quad (7)$$

where the sign makes  $Q_j$  positive in the usual case of scattering four-momenta.

Furthermore, eight distinct internal constituent momenta (in which the subscript refers to the particular

constituent line) appear:

$$\begin{aligned}
k_s &\equiv p_{(sq)} - p_q, \\
k_{\bar{s}} &\equiv p_{[\bar{s}(ud)]} - p_{(ud)}, \\
k_q &\equiv p_{(sq)} - p_s, \\
k_{(ud)} &\equiv p_{[\bar{s}(ud)]} - p_{\bar{s}}, \\
k'_s &\equiv p_\gamma - p'_{\bar{s}}, \\
k'_{\bar{s}} &\equiv p_\gamma - p'_s, \\
k'_q &\equiv p_N - p'_{(ud)}, \\
k'_{(ud)} &\equiv p_N - p'_q,
\end{aligned} \tag{8}$$

which are linearly independent except for the overall momentum conservation constraint. In the full amplitudes  $\mathcal{M}$ , the factors  $\bar{u}_j(p_f)\gamma^\mu(\not{k}_j - m_j)^{-1}\gamma^\nu u_j(p_i)$  appear for the fermionic constituents. By treating the bosonized propagator denominator  $(k_j^2 - m_j^2)$  as the only significant factor for this analysis, *i.e.*, by ignoring the effect of the spinor algebra except to use the Dirac equation of motion to eliminate  $\not{k}_j$  from the numerator, by using the conventional  $2m_j$  normalization for spinors, and by noting that scattering momentum transfers are negative, the relevant dimensionless factors for constituent lines in this analysis are:

$$K_j^{(\prime)} \equiv -\frac{2m_j^2}{k_j^{(\prime)2} - m_j^2}. \tag{9}$$

For convenience, we employ the same form for the (bosonic) diquark constituent ( $ud$ ). From standard relativistic kinematics using Eqs. (3)–(9), one finds that the propagator factors  $Q_s$ ,  $Q_{(ud)}$ ,  $Q_{(sq)}$ ,  $Q_{s\bar{s}}$ ,  $K_{\bar{s}}$ ,  $K_q$ ,  $K'_s$ , and  $K'_q$  are enhanced in the forward direction, while  $Q_{\bar{s}}$ ,  $Q_q$ ,  $K_s$ ,  $K_{(ud)}$ ,  $K'_s$ , and  $K'_{(ud)}$  are enhanced in the backward direction. These results for  $Q_s$ ,  $Q_{(ud)}$ ,  $Q_{\bar{s}}$ ,  $Q_q$  were anticipated in the last section.

The choice of appropriate constituent masses also requires some care. Current quark masses would only be appropriate in a fully perturbative analysis in which classes of diagrams are resummed to avoid singularities associated with particles going on shell. However, traditional constituent masses are not entirely appropriate for this calculation either, as they are typically obtained from static processes, not a dynamical scattering such as photoproduction. The choice of mass parameters, as seen below, lies somewhere in between these extremes.

Even then, the appropriate mass to choose for a given internal constituent line suffers from ambiguity. Take, for example, the factor  $k_q$  in Eq. (8), which refers to the momentum of a light  $q$  emerging from the breakup of the nucleon  $N$  *en route* to binding into a diquark ( $sq$ ). According to Eq. (4), should its mass be considered a fraction  $r_2$  of  $m_N$ , or a fraction  $r_3$  of  $m_{(sq)}$ ? Or indeed, since the propagator lies deep in the diagram, should one use the confinement mass scale  $m_{\text{conf}}$  previously introduced? We adopt the convention that the appropriate effective constituent mass to appear in the propagators Eq. (9) is

the maximum of the two suggested by the initial ( $i$ ) and final ( $f$ ) states into which it binds [according to Eqs. (3) and (4)] *plus* a contribution from the confinement scale  $m_{\text{conf}}$ , to account for the expected off-shell behavior:

$$m_{j,\text{eff}}^2 = \max(m_{j,i}^2, m_{j,f}^2) + m_{\text{conf}}^2. \tag{10}$$

The model amplitudes of Table I in the simplified notation of Eqs. (7) and (9) read

$$\begin{aligned}
\mathcal{M}_1^{(1)} &= Q_s Q_{(ud)} Q_{(sq)} K_{\bar{s}} K_q, \\
\mathcal{M}_2^{(1)} &= Q_s Q_{(ud)} Q_{s\bar{s}} K'_s K'_q, \\
\mathcal{M}_3^{(1)} &= Q_s Q_{(ud)} Q_{\bar{s}} K_q K'_q, \\
\mathcal{M}_4^{(1)} &= Q_s Q_{(ud)} Q_q K_s K'_s, \\
\mathcal{M}_1^{(2)} &= Q_{\bar{s}} Q_q Q_{(sq)} K_s K_{(ud)}, \\
\mathcal{M}_2^{(2)} &= Q_{\bar{s}} Q_q Q_{s\bar{s}} K'_s K'_{(ud)}, \\
\mathcal{M}_3^{(2)} &= Q_{\bar{s}} Q_q Q_{(ud)} K_s K'_s, \\
\mathcal{M}_4^{(2)} &= Q_{\bar{s}} Q_q Q_s K_{(ud)} K'_{(ud)}, \\
\mathcal{M}_1^{(3)} &= Q_q Q_{(ud)} Q_{(sq)} K_s K_{\bar{s}}, \\
\mathcal{M}_2^{(3)} &= Q_s Q_{\bar{s}} Q_{(sq)} K_q K_{(ud)}, \\
\mathcal{M}_3^{(3)} &= Q_{\bar{s}} Q_{(ud)} Q_{s\bar{s}} K'_s K'_q, \\
\mathcal{M}_4^{(3)} &= Q_s Q_q Q_{s\bar{s}} K'_s K'_{(ud)}.
\end{aligned} \tag{11}$$

The chosen input masses, all in MeV, are listed in Table II. Again, guidance for this choice is suggested, but not determined, by an interpolation between typical current and constituent masses used in the literature. For example, one can make an argument for ( $ud$ ) diquark masses anywhere from  $\simeq 30$  MeV (*i.e.*, not many times more than the sum of current quark masses) up to  $\simeq 600$  MeV (*i.e.*, two-thirds of a nucleon, or the mass of a  $\sigma$  meson). The most important inputs in obtaining a re-

TABLE II: Input masses in MeV.

$\sqrt{s}$	$m_\gamma$	$m_N$	$m_{(sq)}$	$m_{[\bar{s}(ud)]}$	$m_{(ud)}$	$m_s = m_{\bar{s}}$	$m_q$	$m_{\text{conf}}$
2200	0	938.3	680	1150	100	200	10	425

sult resembling experimental data appear to be choosing  $m_{(sq)} + m_{[\bar{s}(ud)]}$  not terribly far below the observed forward peak at  $\sqrt{s} = 2.2$  GeV, and choosing a fairly large value for  $m_{\text{conf}}$ . The necessary magnitude of  $m_{\text{conf}}$  appears to arise largely due to the feature of this simplified model that the initial  $s$  and  $\bar{s}$  quarks from the dissociation of  $\gamma$  are lightlike, as seen from the first two of Eq. (4); presumably, introducing substantial transverse momenta in a more realistic calculation produces the same effect as  $m_{\text{conf}}$ . In any case, the model presented here is so simple that the input masses used should be viewed only as a qualitative guide to obtaining results in accord with experiment.

For the given inputs, the amplitudes of class  $\mathcal{M}^{(1)}$  are all strongly peaked in the forward direction, while those

of class  $\mathcal{M}^{(2)}$  are all strongly peaked in the backward direction but possess in addition a smaller forward peak. In particular, the amplitude  $\mathcal{M}_1^{(1)}$  [ $\mathcal{M}_1^{(2)}$ ] corresponding to Fig. 3 (Fig. 4) shows preferential forward (backward) scattering, as was anticipated from general arguments. The diagrams of class  $\mathcal{M}^{(3)}$  also turn out to be forward enhanced, but many times smaller than those in class  $\mathcal{M}^{(1)}$ . To illustrate the forward-backward peaking, we present in Fig. 6 the simple coherent sum  $M$  of the 12 amplitudes. Obviously, the absence of numerous factors

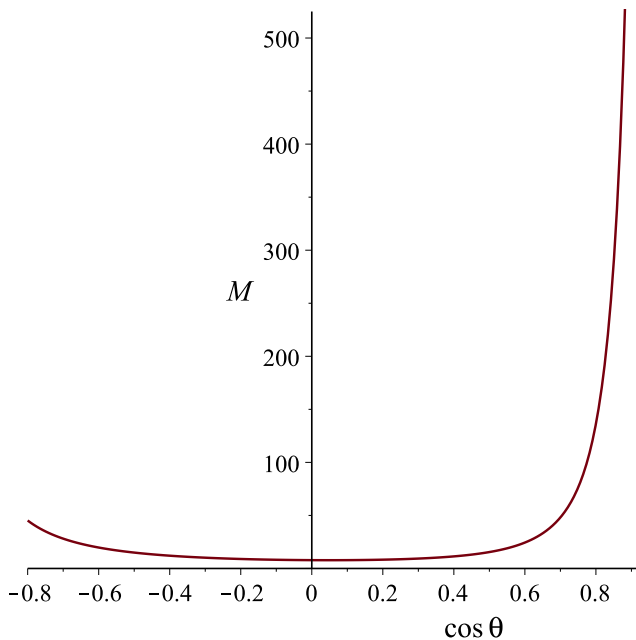


FIG. 6: Coherent sum  $M$  of the 12 amplitudes of Eq. (11) using the inputs in Table II, as a function of  $\cos \theta$ .

in the full Feynman amplitudes—not least of which are relative signs leading to destructive interferences—means that the plot of Fig. 6 should only be taken seriously in its coarsest features, namely, a large peak in the forward direction and a small peak in the backward direction. The particular value for the forward-to-backward ratio is simple to adjust using slightly different inputs. Furthermore, we note that the CLAS data presented in Ref. [10] does not extend to the most forward and backward directions; the limitation  $-0.80 \leq \cos \theta \leq +0.92$  is used in Fig. 6. The literal ratio  $M(\cos \theta = +0.92)/M(\cos \theta = -0.8)$  in Fig. 6 is about 30.

Lastly, one may ask whether the forward enhancement behaves away from the particular chosen peak value  $\sqrt{s} = 2.2$  GeV similarly to its appearance in the data. To illustrate the result, we plot in Fig. 7 the amplitude  $\mathcal{M}_1^{(1)}$  as a function of  $\sqrt{s}$  but otherwise use the mass inputs of Table II. The amplitude, rather than its square, is relevant because its chief contribution to data would presumably appear through interference with the dominant Pomeron amplitude. The full width at half max-

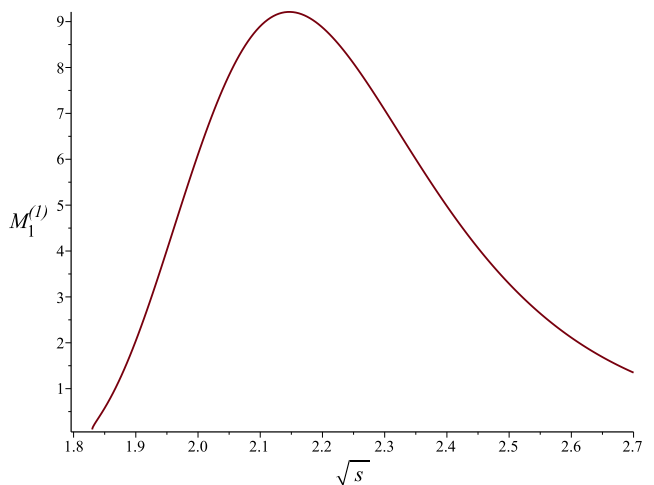


FIG. 7: Behavior of the amplitude  $\mathcal{M}_1^{(1)}$  as a function of  $\sqrt{s}$  (in GeV), with the other inputs as in Table II.

imum appears to extend from just below 2.0 GeV to about 2.4 GeV, which is very much like the experimental result presented in Refs. [10, 12]. In this model, the enhancement is indeed due to a special correlated five-quark configuration, but it is not a literal resonant pentaquark state. That is, the anomalies may be said to correspond to “would-be” pentaquarks.

## V. CONCLUSIONS

We have seen that interesting forward-backward enhancements observed in recent data for the photoproduction process  $\gamma p \rightarrow \phi p$  can easily be explained through the production of a  $(su)$  color- $\bar{\mathbf{3}}$  bound diquark and an  $[\bar{s}(ud)]$  color- $\mathbf{3}$  bound antitriquark, using the preferential color couplings  $\mathbf{3} \otimes \mathbf{3} \supset \bar{\mathbf{3}}$ . Such a configuration (with  $s \rightarrow c$ ) has previously been advocated as an explanation of the exotic charmoniumlike states. Here, however, no claim is made that the enhancements are the result of true resonances, but they are predicted to create  $s$ -dependent bumps in the data.

The model relies only on the preference of a system with largely collinear constituents to minimize the constituent momentum transfers. Essentially no dynamics is included; the minimal set of gluon exchanges used for each diagram does not incorporate color physics in any fundamental way. Likewise, the constituents are assumed at any point in the diagrams to carry only momenta parallel to the bound state in which they occur. Nevertheless, using plausible values for constituent masses, one obtains results in good qualitative, and even semi-quantitative, agreement with experiment. Numerous possible improvements leading to stable and predictive results for this process should certainly be undertaken.



The possibility that diquark/triquark structure can be discerned in lighter quark systems has long been discussed, but the experimental signals have always been tantalizingly vague. In the analogues to the types of experiments already performed or proposed for heavy-quark exotics, one can hope to find a clear indication for these novel structures.

### Acknowledgments

I gladly acknowledge M. Karliner for a conversation on his recent paper, which ultimately inspired the idea for

this work. I also thank S. Brodsky for providing perceptive comments, M. Dugger for generating detailed plots of CLAS data, and the CERN Theoretical Physics Group for support during this work's completion. This work was supported by the National Science Foundation under Grant Nos. PHY-1068286 and PHY-1403891.

- 
- [1] R. Aaij *et al.* [LHCb Collaboration], *Phys. Rev. Lett.* **115**, 072001 (2015) [arXiv:1507.03414 [hep-ex]].
  - [2] S.J. Brodsky, D.S. Hwang, and R.F. Lebed, *Phys. Rev. Lett.* **113**, 112001 (2014) [arXiv:1406.7281 [hep-ph]].
  - [3] S.H. Blitz and R.F. Lebed, *Phys. Rev. D* **91**, 094025 (2015) [arXiv:1503.04802 [hep-ph]].
  - [4] R.F. Lebed, *Phys. Lett. B* **749**, 454 (2015) [arXiv:1507.05867 [hep-ph]].
  - [5] M. Karliner and H.J. Lipkin, *Phys. Lett. B* **575**, 249 (2003) [hep-ph/0402260].
  - [6] R.F. Lebed, arXiv:1508.03320 [hep-ph]. Presented at CHARM-2015, Detroit, MI, 18–22 May 2015.
  - [7] Q. Wang, X.H. Liu, and Q. Zhao, *Phys. Rev. D* **92**, 034022 (2015) [arXiv:1508.00339 [hep-ph]].
  - [8] V. Kubarovsky and M.B. Voloshin, *Phys. Rev. D* **92**, 031502 (2015) [arXiv:1508.00888 [hep-ph]].
  - [9] M. Karliner and J.L. Rosner, arXiv:1508.01496 [hep-ph].
  - [10] B. Dey *et al.* [CLAS Collaboration], *Phys. Rev. C* **89**, 055208 (2014) [*Phys. Rev. C* **90**, 019901 (2014)] [arXiv:1403.2110 [nucl-ex]].
  - [11] K.P. Adhikari *et al.* [CLAS Collaboration], *Phys. Rev. C* **89**, 055206 (2014) [arXiv:1308.1363 [hep-ex]].
  - [12] B. Dey, arXiv:1403.3730 [hep-ex].
  - [13] W.R. Gibbs and B. Loiseau, *Phys. Rev. C* **50**, 2742 (1994).
  - [14] M.E. McCracken *et al.* [CLAS Collaboration], *Phys. Rev. C* **81**, 025201 (2010) [arXiv:0912.4274 [nucl-ex]].
  - [15] P.G.O. Freund, *Nuovo Cimento* **48A**, 541 (1967).
  - [16] V.D. Barger and D. Cline, *Phys. Rev. Lett.* **24**, 1313 (1970).
  - [17] A. Goritschnig, B. Melic, K. Passek-Kumericki, and W. Schweiger, *PoS DIS* **2014**, 170 (2014) [arXiv:1411.0904 [hep-ph]].
  - [18] C.E. Carlson, C.D. Carone, H.J. Kwee and R.F. Lebed, *Phys. Lett. B* **635**, 100 (2006) [hep-ph/0512207].
  - [19] G.F. de Teramond, H.G. Dosch, and S.J. Brodsky, *Phys. Rev. D* **91**, 045040 (2015) [arXiv:1411.5243 [hep-ph]].
  - [20] H.G. Dosch, G.F. de Teramond, and S.J. Brodsky, *Phys. Rev. D* **91**, 085016 (2015) [arXiv:1501.00959 [hep-th]].
  - [21] J.F. Gunion, S.J. Brodsky and R. Blankenbecler, *Phys. Rev. D* **8**, 287 (1973).
  - [22] J.R. Forshaw, R. Sandapen and G. Shaw, *Phys. Rev. D* **69**, 094013 (2004) [hep-ph/0312172].
  - [23] A.V. Efremov and A.V. Radyushkin, *Phys. Lett. B* **94**, 245 (1980).
  - [24] G.P. Lepage and S.J. Brodsky, *Phys. Rev. D* **22**, 2157 (1980).
  - [25] S.J. Brodsky, H.C. Pauli and S.S. Pinsky, *Phys. Rept.* **301**, 299 (1998) [hep-ph/9705477].